

Nonlinear characteristics of high amplitude focusing using time reversal in a reverberation chamber

Brian D. Patchett and Brian E. Anderson

Citation: [The Journal of the Acoustical Society of America](#) **151**, 3603 (2022); doi: 10.1121/10.0011517

View online: <https://doi.org/10.1121/10.0011517>

View Table of Contents: <https://asa.scitation.org/toc/jas/151/6>

Published by the [Acoustical Society of America](#)



**Advance your science and career
as a member of the**

ACOUSTICAL SOCIETY OF AMERICA

LEARN MORE



Nonlinear characteristics of high amplitude focusing using time reversal in a reverberation chamber

Brian D. Patchett  and Brian E. Anderson^{a)} 

Acoustics Research Group, Department of Physics and Astronomy, Brigham Young University, Provo, Utah 84602, USA

ABSTRACT:

Time reversal (TR) signal processing is an effective tool to exploit a reverberant environment for the intentional focusing of airborne, audible sound. A previous room acoustics TR study found preliminary evidence that above a certain focal amplitude the focal waveform begins to display signs of nonlinearity [Willardson, Anderson, Young, Denison, and Patchett, *J. Acoust. Soc. Am.* **143**(2), 696–705 (2018)]. This study investigates that nonlinearity further by increasing the focal peak amplitudes beyond that previously observed. This increases the nonlinear characteristics, allowing for a closer inspection of their properties. An experiment is conducted using eight horn loudspeaker sources and a single receiver in a reverberation chamber. A maximum peak focal amplitude of 214.8 kPa (200.6 dB_{pk}) is achieved. The focus signal waveforms are linearly scaled to observe and characterize the nonlinear amplification of the waveform. Frequency spectra of the peak focal amplitudes are plotted to observe changes in frequency content as the signals become nonlinear. A one-dimensional spatial scan of the focal region is conducted to observe properties of the converging and diverging waves. A proposal for a possible explanation involving free-space Mach stem formation is given. © 2022 Acoustical Society of America. <https://doi.org/10.1121/10.0011517>

(Received 21 February 2022; revised 11 May 2022; accepted 12 May 2022; published online 1 June 2022)

[Editor: Julian D Maynard]

Pages: 3603–3614

I. INTRODUCTION

Time reversal (TR) is a signal processing technique utilized in multiple areas of wave physics.^{1–3} Its origins began in the early 1960s to provide reproducible sound transmission for underwater communication,^{4,5} and at the time was referred to as matched signal processing. TR has been used in a reverberant environment to generate intentional focusing of sound at a receiver position from a distant source, or bank of sources.^{6–9} There is a forward step, and a backward step when generating a TR focus. In the forward step an impulse response (IR) is obtained for a physical system. To accomplish this, a chirp signal is broadcast from a source position and the response is recorded at a receiver position as the chirp response (CR). The IR can then be approximated by performing a cross correlation of the original input chirp signal and the CR.^{10,11} In the backward step, the IR is reversed in time [afterward referred to as the time-reversed impulse response (TRIR)] and broadcast from the source position. Due to the reciprocity of the system, the TRIR produces waves that retrace the same paths traversed during the forward step, resulting in acoustic waves converging on the receiver position as a focus of sound.

There are a wide variety of applications of high-amplitude TR. One such area, non-destructive evaluation of solid materials, utilizes TR to probe solid materials with focused ultrasound at various locations to locate and image defects in the solid by observing nonlinear content of the resulting focus signal.^{3,12–18} The TR focusing generated in these studies is large enough to excite nonlinear wave

motion of cracks or delaminations in the material, but not high enough amplitude to induce nonlinear motion of the intact portions of the material. Through a relative comparison of the TR focusing generated at intact and damaged locations, one can identify the damaged locations by observing relative increases in nonlinear wave phenomena (e.g., harmonic frequency content). Additional analytical methods have also been developed to help increase the ability to detect nonlinearities when TR is focused at localized positions in a solid. These include phase inversion (or pulse inversion),^{14,18} the scaling subtraction method (implemented in the time domain^{12,13} and the frequency domain^{12,16,17}), and third-order phase symmetry analysis.¹⁹ Observation of nonlinearities in TR focused waves in solid materials without localized defects, such as in concrete mortar blocks, has been made but not carefully studied.²⁰ Several of the methods listed above were found to be of use in interpreting the data presented in this paper.

High amplitude TR has multiple biomedical applications as well. In a paper by Thomas *et al.*,²¹ the treatment of kidney stones, known as lithotripsy, is discussed as an application where a time-reversal mirror (in the form of a small transducer array) is used to target a kidney stone. Studies of the application of TR for histotripsy applied to brain tumor treatment have also been conducted.^{22,23} These studies applied the methods of TR to focusing through inhomogeneous materials to multiple positions within a human skull. TR has also been used as a method of imaging imperfections in human teeth using ultrasound.²⁴ In each of these papers the goal was to generate high amplitude acoustic energy rather than to study any nonlinearities of the focused waves.

^{a)}Electronic mail: bea@byu.edu

The use of TR in room acoustics initially explored communications applications in complex environments.^{6–9} Ribay *et al.*⁸ asserted that in an average room environment the amplitude of the TR focusing is proportional to the number of sources, reverberation time of the room, and bandwidth of the impulse response. Denison and Anderson²⁵ confirmed that a longer reverberation time leads to a higher focal amplitude if the reverberation time is altered due to changes in the absorption in the room. However, they found that increasing the room size to increase the reverberation time decreased the amplitude of TR focusing. Denison and Anderson²⁶ also found that sources used in the backward step should be placed further away from the focusing location than the critical distance in the room and that sources and focusing location should be in the same Cartesian plane in a rectangular room. Anderson *et al.*¹¹ showed that, in a reverberant room, aiming sources away from the intended location for TR focusing also increases the amplitude of the focus. Willardson *et al.*²⁷ explored the use of TRIR modification methods and found that the processing technique known as clipping yielded the largest amplitude TR focusing. Using the clipping technique, they were able to achieve a peak focus sound pressure level of 173.1 dB_{pk} using a chirp with a bandwidth of 500–7500 Hz. Wallace and Anderson²⁸ demonstrated that TR focusing of airborne ultrasound could be used to generate a nonlinear difference frequency, achieving peak focal amplitudes of 134 dB_{pk} [henceforth, all measured dB values are peak values (dB_{pk}) reported with a reference of 20 μPa] with frequencies between 35 and 40 kHz. And recently, Patchett *et al.*²⁹ showed that the amplitude of the TR focusing depends on the location of the receiver with respect to the room boundaries. Placing the microphone used to measure the IR(s) in the corner of the room in order to focus sound there yields approximately a 9 dB increase in the focusing amplitude compared to the microphone being placed away from all walls in the room.

Appert *et al.*³⁰ presented an analytical and numerical study applied to observations of nonlinear wave steepening in the generation of nucleation points in liquid helium via the use of focused spherical sound waves. While TR was not used in this case, the observations of nonlinearities in a focused sound wave prove relevant to this study. The models used indicated that the breakdown of the standard linear equation of state for helium was a key factor in the generation of nonlinearity in that study. Nonlinear behavior in TR focusing of underwater sound was also observed in a study by Montaldo *et al.*³¹ They showed that when focal signals are generated underwater with increasing amplitude the wave distorts in shape, in that the leading side of a compression peak in a focus signal steepens significantly forming shock waves. When the results of Montaldo *et al.* are linearly scaled, the amplitude of the largest compression peak is lower in amplitude than the linearly scaled version of the lower amplitude focus signal. Their experimental setup had waves propagating principally from one direction to the focus location, whereas in this paper the wave focusing effectively comes from all directions (when including the

contributions from image sources). Willardson *et al.*²⁷ demonstrated that TR can be used to generate high amplitude acoustic focusing in air. At the maximum focusing amplitudes they reported of 173 dB_{pk}, there was an observable distortion in the focus signal. This distortion was characterized by steepening of the leading edge of the focus in the time domain, a slight nonlinear increase in the amplitude of compressions, and a slight nonlinear suppression of rarefactions. This nonlinear increase in focused compressions observed by Willardson *et al.* in airborne focusing was not observed by Montaldo *et al.* with underwater focusing; instead, compression peaks decreased in the Montaldo *et al.* study. Wallace and Anderson²⁸ did not observe wave steepening or these nonlinear increases and suppressions of compressions and rarefactions, respectively.

The purpose of this paper is to further study the nonlinearities apparent in TR focusing of higher amplitudes than those achieved by Willardson *et al.* Higher amplitudes are achieved by using a smaller reverberation chamber, multiple high-amplitude loudspeakers in the same plane as the focusing location, pointing the sources away from the focal location, using the clipping TR method, and focusing in the corner of the room. As summarized previously each of these methods contributes to higher amplitude focusing. Importantly, microphones with lower sensitivities than those used by Willardson *et al.* were used here to enable accurate recording of these higher amplitudes. These measures allow the generation of TR focusing amplitudes that greatly exceed any previously measured results, thereby increasing the nonlinearities in the focused waves allowing a more careful observation of them. Comparisons of linearly scaled focal signals are presented, as well as a one-dimensional spatial scan of the high-amplitude converging and diverging waves of the TR process. Optimization of the amplitude of the TR focusing is discussed, with a description of the applied methods of refinement. A comparison of different microphone types is done to confirm that the levels reached are genuine and not an artifact of the equipment or systematic error. Representation of the harmonic content is also presented to show that the high frequency content increases significantly as the focus amplitude is increased. A proposed explanation of the observed nonlinearities is presented, that of free-space, Mach-wave generation in the superposition of converging waves.

II. EXPERIMENTAL DETAILS

A. Setup

The experiments were carried out in the smaller of two reverberation chambers available on the campus of Brigham Young University. This is due to the findings by Denison and Anderson²⁵ and by Patchett *et al.*²⁹ showing that a room of smaller volume and dimension contributes to a higher peak focal amplitude. This smaller reverberation chamber has dimensions 5.7 m × 4.3 m × 2.5 m and a volume of 61 m³. The overall reverberation time in the room is approximately 4.16 s across the chirp bandwidth used, with a

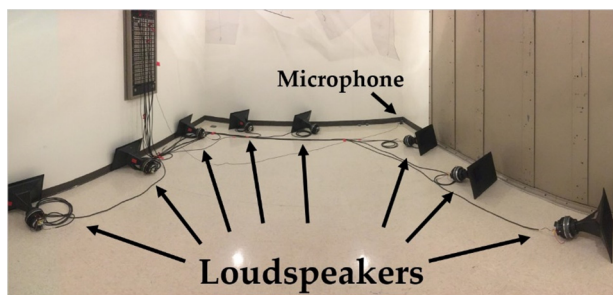


FIG. 1. (Color online) Photograph of the experimental layout in the small reverberation chamber. The room is a rectangular room with parallel walls, along with diffusing panels (partially shown at the top of the image) intended to make the sound field more diffuse. Distortion in the image is due to the panoramic nature of the photograph.

Schroeder frequency of 522 Hz. While the large chamber used measures 4.96 m × 5.89 m × 6.98 m, with a volume of 204 m³, with an overall reverberation time of 7.6 s across the chirp bandwidth, and a Schroeder frequency of 410 Hz. A PCB (Buffalo, NY) microphone, model 112A21 with a sensitivity of 7.1 mV/kPa, is the primary receiver for the experiments unless otherwise stated. It is placed in the lower corner of the chamber and oriented pointing toward the floor, with the face 1 cm from each adjacent wall. Eight BMS (Hannover, Germany) 4590 dual diaphragm high output loudspeakers fitted with the appropriate crossovers and horns manufactured by BMS are utilized as the sources (referred to as loudspeakers). A photograph of the setup is shown in Fig. 1. They are placed in the chamber facing toward the walls in order to minimize the amplitude of the direct acoustic path to the microphone.¹¹ When utilizing normalized TRIRs, the TR process yields higher amplitude focusing when the direct sound is not much larger than the multi-path reverberation in the TRIR. This is achieved by

pointing somewhat directional sources away from the target microphone for the focusing location so that the direct sound arrival is smaller in amplitude. Power to the drivers is provided by two Crown (Elkhart, IN) CT4150 amplifiers. A swept sine wave (chirp signal) is then created with a bandwidth of 500–15 000 Hz, and length of 4.16 s. This chirp is broadcast sequentially from each driver. This allows for a calculation of the IR for each individual loudspeaker-to-microphone combination.

The preprocessing method known as clipping is applied to the TRIR signals before they are broadcast during the backward step. This method has been shown to be the most effective at increasing the focus amplitude, in both air and in solid media, when compared to other well-known methods of preprocessing.^{27,32} Clipping TR, similar in nature to one-bit TR,³¹ intentionally clips the higher amplitude portions of a TRIR, which is then normalized, resulting in a relative increase in the broadcasted energy. Importantly, the phase information (timing of the reflections) is preserved in the TRIR. The threshold value for clipping in these experiments was set to 0.05. This value is slightly different than the threshold used by the Willardson *et al.* but was found to optimize peak focus amplitudes in various trials during the experimental setup and calibration. These clipped TRIRs are normalized to utilize the full power output available from the amplifiers. The TR process is carried out using an in-house designed LABVIEWTM (Austin, TX) executable program, coupled with two Spectrum Instrumentation (Großhansdorf, Germany) M2i.6022 signal generation cards and a M2i.4931 digitizer card. A sampling frequency of 250 kHz is used for generating and digitizing all signals used in this study. All post-processing is done with MATLABTM (Natick, MA). Figure 2 shows an example of the signals generated in the TR process used here.

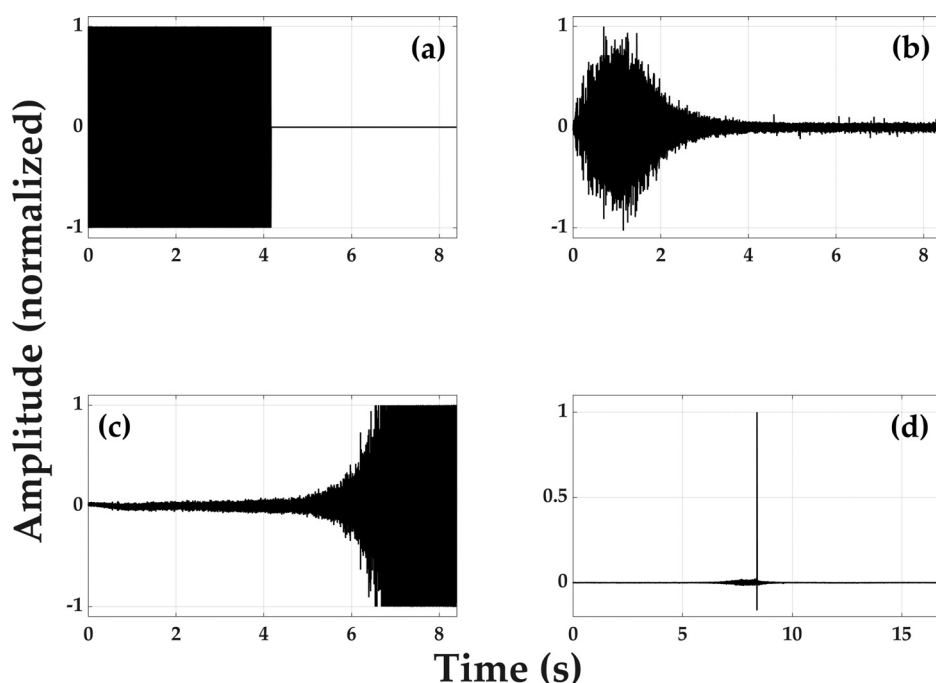


FIG. 2. Example signals used in the time reversal experiments. (a) The logarithmic, swept-sine chirp signal. (b) The chirp response (CR) recorded in the forward step at the microphone. (c) The normalized, clipped time reversed impulse response (TRIR). (d) Focus signal generated by simultaneous broadcast of eight loudspeakers. All amplitudes in this figure are normalized.

B. Linear vs logarithmic chirp signal

The use of a cross correlation of the chirp signal and measured CR to extract an IR typically relies on the use of a linearly varying, swept-sine frequency chirp (linear chirp). It is logical to assume that equal amplitude per frequency will produce the optimal amount of amplitude in TR focusing of impulsive signals since a Delta function's spectrum contains equal amplitude at all frequencies. However, it was found empirically by others (including the authors) in a few different systems that the use of a logarithmically varying, swept-sine frequency chirp (log chirp) yielded larger TR focusing amplitudes than when using a linear chirp.^{27,28,33} Higher frequencies generally experience a larger degree of damping with wall absorption, thermo-viscous propagation, and boundary-layer losses. This results in a frequency-dependent reverberation time in the room, with longer reverberation times at lower frequencies. Therefore, the use of a log chirp, with a longer time spent at lower frequency, will result in an IR with overall longer reverberation times than would be found when using a linear chirp because there is more low frequency content. Longer reverberation times in the IRs results in larger amplitude TR focusing for a given room.⁸

Figure 3 shows a comparison of the IR time signals and their corresponding spectra. The IRs are normalized by their respective peak values but the frequency spectra are both normalized with respect to the peak of the log spectrum.

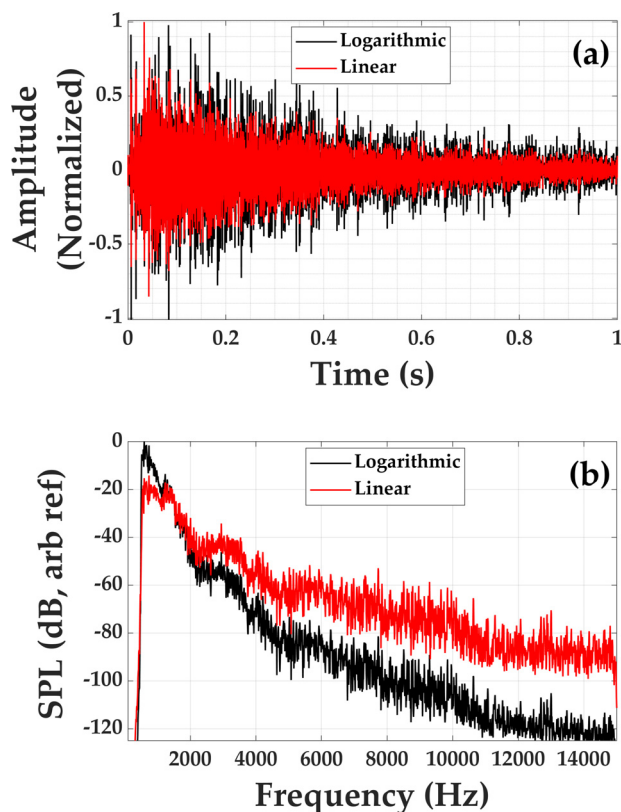


FIG. 3. (Color online) Normalized (a) impulse response signals and (b) associated frequency response spectra obtained with linear and log chirp signals (both normalized with respect to the peak of the logarithmic spectrum).

While similar in amplitude over time, the IR obtained with the log chirp has a larger amount of energy over the time period shown. The spectrum of the IR obtained with the log chirp also has a larger amount of energy present at low frequencies. Overall energy can be compared by squaring and then summing the pressure sample values in the IR signals. This method of energy comparison reveals an energy increase in the log signal of 12 dB compared to the linear signal, which indicates average pressure values are four times higher in the log IR when compared to the linear IR (Fig. 3). Due to the higher overall energy in the normalized IR obtained with the log chirp, application of clipping TR should also benefit from the use of the log chirp in terms of achieving a larger focusing amplitude. This is because a larger amplitude exists for a longer period of time in the TRIR so that when it is clipped more energy remains in the clipped TRIR and thus more energy is broadcast in the backward step. Empirical results demonstrate that the use of a log chirp to obtain the IR results in a larger TR focusing amplitude whether clipping TR is used or not. Based on these results a log chirp is used throughout the remainder of the experiments.

III. GENERATING A HIGH-AMPLITUDE FOCUS

A. Physical nonlinear characteristics

The TR process is now optimized to achieve the maximum possible peak focal amplitude by using a logarithmic chirp, eight loudspeakers, the clipping TR method, a smaller reverberation chamber, and by placing the microphone in a corner position. The peak focal amplitudes now obtained greatly exceed levels that have previously been reported for TR focusing of sound in air. The focal signals are modified in order to scale their amplitudes linearly up to the highest amplitude result, allowing for analysis of the focusing waveform as the output level is increased. By scaling the signals in this manner, a comparison of the nonlinear departure from linear scaling can be made. Figure 4 shows a zoomed-in view of the focal signals at the microphone location at five different levels. The same TRIRs were used in each case but the amplitude of the input signals to the amplifiers were increased. As the output from the generating cards is increased there is a dramatic change in the focal waveforms. The leading edge steepens dramatically, moving the largest compression peak forward in time. This is an indication of an amplitude dependence of the speed of sound. The rarefactions shift backward in time, indicating a relative slowing of their propagation speed. These amplitude-dependent, wave-steepening observations are characteristic of nonlinear shock wave formation.³⁴⁻³⁶ The peak focus value for the highest amplitude focus signal in Fig. 4(a) measures 214 800 Pa, a sound pressure level of 200.6 dB_{pk}. Atmospheric pressure at the elevation where these measurements were made is 86 kPa, not the standard 101 kPa at sea level. This means that the peak pressure of 215 kPa is approximately 2.4 times the ambient pressure, or an overpressure that is 1.4 atmospheres above the ambient pressure.

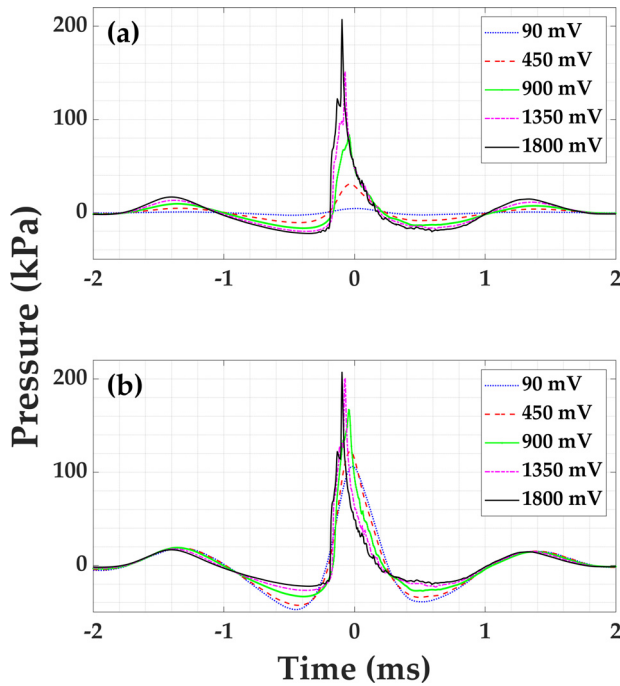


FIG. 4. (Color online) (a) Five focus signals recorded at the microphone position as the voltage of the signal from the generator cards is increased. (b) Linearly scaled versions of the focus signals in (a). Legend values represent the output level from the generator cards.

Figure 4(b) compares the same waveforms as shown in Fig. 4(a) but these are linearly scaled by multiplying each signal by the appropriate scaling constant relative to the scaling used for the output voltage signal amplitude. This figure illustrates the primary nonlinear phenomenon of interest. When scaled, linear waveforms should be identical with small deviations being possible due to background noise. In Fig. 4(b) it is apparent that the large compression peak increases in amplitude in a nonlinear fashion. Smaller effects were reported by Willardson *et al.*²⁷ The compression peak distorts significantly in shape by steepening on the leading edge of the compression. There are two peaks evident in the compression peak and the presence of both of these peaks is repeatable in these largest amplitude experiments. The initial, lower amplitude peak is caused by a prominent wave (sidelobe) that is detected by the microphone prior to it reflecting off of the nearby wall and arriving at the intended focal time. The trailing edge of the compression peak rolls off in amplitude more slowly than linear scaling would predict. The rarefactions on either side of the compression peak also do not scale linearly. These rarefactions are nonlinearly suppressed with increasing amplitude of the focusing. The lower amplitude peaks and troughs at times before and after these rarefactions appear to maintain linear scaling. This suggests that only in the high enough amplitude waves that produce the TR focusing are these nonlinear effects observed. Additionally, because the lower amplitude peaks before and after the main focal event scale linearly, this suggests that the distortion is generated acoustically rather than by the amplifiers since the distortion of the peaks only occurs for the higher amplitude peaks.

Multiplication of the TRIR signals by -1 inverts the phase of these signals and when used in the TR process this creates a focused rarefaction as opposed to a compression. The results of this inversion, shown in Fig. 5, was done to observe the nonlinear effects seen when the focus is a rarefaction as opposed to a compression (Fig. 4). It is apparent from Fig. 5 that similar physical phenomena are present in a rarefaction focus as well. The scaled rarefaction focus also exhibits a suppression of its maximum and is shifted later in time. The leading and trailing compressions show nonlinear growth with increasing amplitude. Instead of wave steepening happening on the leading edge of the compression, as observed with a focused compression, now a wave steepening is observed most dramatically on the trailing edge of the rarefaction peak, which is the leading edge of the largest compression peak. The lowest peak rarefaction value measured is 31 300 Pa (in absolute units), a value of 54 700 Pa (underpressure) below the ambient level of 86 kPa, or a sound pressure level of 188.7 dB_{pk}.

B. Frequency analysis of focus signals

An autospectrum of each increasing-amplitude focus signal from Fig. 4 provides insight into the changes in the frequency content as the focal signal amplitude increases and subsequent acoustic nonlinearity increases. Figure 6 shows that as the level of the input signal is increased, the low frequency content decreases, and the high frequency content increases. A similar analysis of the frequency content of the focal signals was made in the Willardson *et al.*

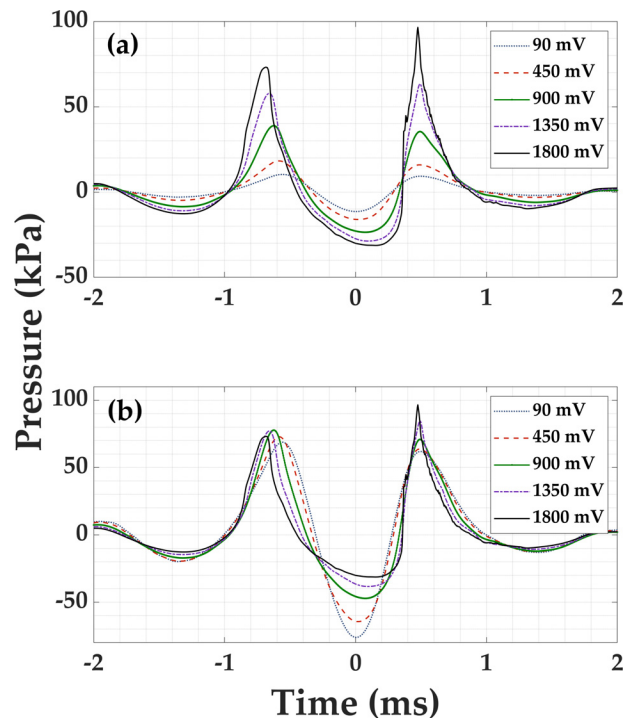


FIG. 5. (Color online) (a) Five inverted focus signals recorded at the microphone position as the voltage of the signal from the generator cards is increased. (b) Linearly scaled versions of the inverted focus signals in (a). Legend values represent the output level from the generator cards.

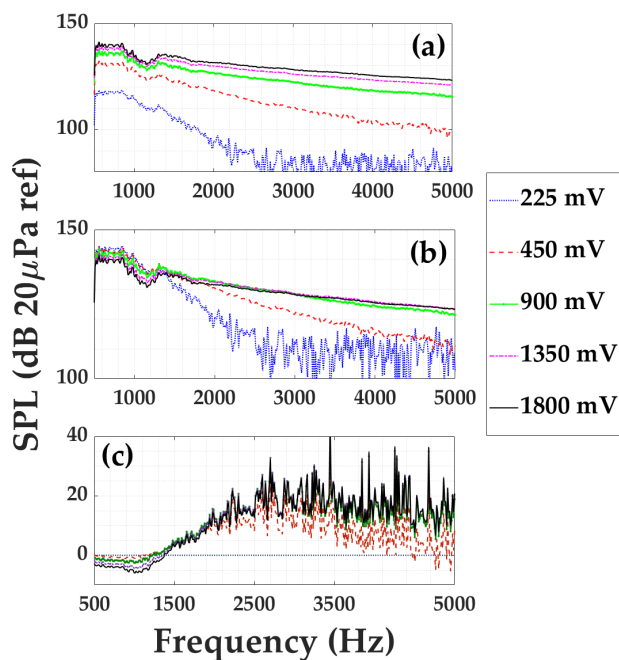


FIG. 6. (Color online) (a) The autospectrum of each focus signal of Fig. 4 with increasing output from the generator cards. (b) The scaled autospectrum of each focus. (c) The difference of the scaled autospectra in (b) with respect to the lowest amplitude spectrum.

study of this phenomenon.²⁷ Figure 6(c) depicts the auto-spectral difference in the focus signal recorded by the microphone as the gain is increased (relative to the lowest amplitude spectrum). It is apparent from Fig. 6(c) that there is a large increase in the high frequency content extending from 1500 to 7500 Hz when the focus signal amplitude is increased. The presence of increasing high frequency content is an indicator that the focus signal may be developing harmonic content that is characteristic of nonlinear harmonic generation as the waves steepen due to high amplitude propagation of the waves. Typically, with nonlinear acoustic harmonic generation of a sine wave, the higher harmonics grow in amplitude as the amplitude of the fundamental decreases and the overall peak amplitude of the wave decreases.³⁴ This would suggest that the peak focal amplitudes observed should decrease as the acoustic amplitude of the focus increases. However, as shown in Fig. 4, there is a nonlinear increase in the peak amplitude of the focus, while the high frequency content continues to increase. In the linearly scaled spectra plot [Fig. 4(b)] frequencies between 500 and 1000 Hz of the highest amplitude focus spectrum loses 6 dB, while the frequencies from 1000 to 2000 Hz see an increase by as much as 10 dB, when compared to the lowest level peak focus amplitude. It appears that the high frequency content begins to converge to a constant increase value as the focal signal amplitude is increased. The large fluctuations seen in the high frequencies (above 2500 Hz) of the lowest focal amplitude signal in Fig. 4(c) are due to the recording being near the noise floor of the microphone. Thus, the differences in the higher amplitude spectra should be greater than those displayed in

Fig. 4(c), likely continuing to increase at the slope seen from 1500 to 2500 Hz.

C. Confirmation of focus amplitude values using multiple microphones

To the authors' knowledge, the peak levels produced in this study far exceed any achieved in previously conducted experiments of TR with airborne sound, being 29.5 dB higher than the peak level reported by Willardson *et al.*²⁷ It is also noteworthy that the peak levels measured exceed the operating limits of most condenser microphones. An investigation into the validity of the amplitude values measured by the equipment is conducted using two different microphones measuring the same TR focusing events. As is demonstrated in Sec. IV, the spatial width of the peak is on the order of 1 cm. This allows for two microphones to be placed closely enough to measure the same focus amplitude with relative accuracy. A PCB (Depew, NY) 112A21 and a GRAS (Holte, Denmark) 46BG are used to conduct the test. The 112A21 is a piezoelectric-type transducer designed to measure high-amplitude pressure waves, with a manufacturer's specified measurement maximum level of 210 dB, and sensitivity of 7.10 mV/kPa. The 46BG is an electret, condenser microphone (pressure type) with a measurement maximum level of 184 dB and sensitivity of 300 mV/kPa. The forward step of recording the chirp response was done with the 112A21. Because of its lower sensitivity level, the frequency content stays well within the measurable range of the 46BG, and no loss of frequency content need be assumed due to the difference in the two microphones differing sensitivities. For this test, the microphones were placed in the middle of the small reverberation chamber oriented with the faces of the diaphragms toward each other, and a spacing between them of about 3 mm.

The measurements were done by beginning with a minimum output level from the Spectrum generator cards of 100 mV, and then incrementally increasing that level by 3 dB until the peak focal amplitude reached the maximum operating level of the 46BG. Each focus was performed five times to obtain an average value for each measurement. In order to demonstrate that the measurements from each microphone are very closely matched, the experiment is initially done with just one source loudspeaker. This resulted in focal amplitudes that are low enough that nonlinear characteristics are not observable in the focus signal. The experiment is then repeated with all eight of the sources, and the levels are increased until the 46BG reaches its maximum operating limit (here, 1131 mV output from the generator cards). Figure 7 illustrates the values recorded by each microphone. The magnitudes for the maximum rarefactions (the maximum negative value just prior to the peak compression) of the focus signals is also plotted. This demonstrates that the peak focus amplitudes reached throughout these measurements are being reliably measured, and no acoustic nonlinearity differences or microphone distortions are present. The two microphones have two very different types of transduction mechanisms and since both report the

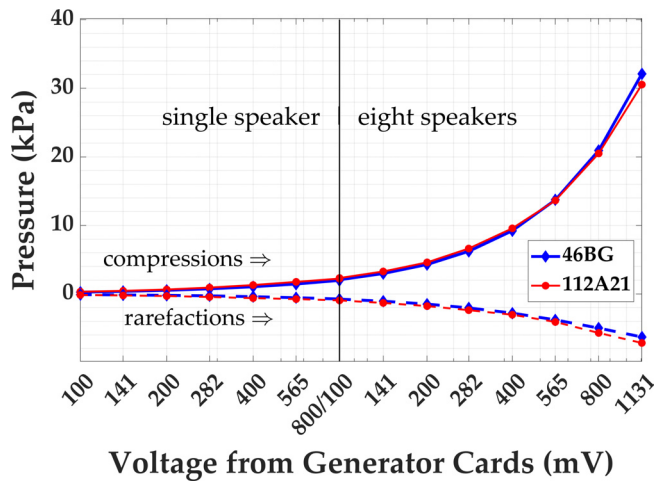


FIG. 7. (Color online) Comparison of PCB 112A21 and G.R.A.S. 46BG simultaneous microphone measurements of the same focus events as the output levels from the generator cards are increased.

same peak amplitudes, it can be assumed that no microphone distortions are present since it would be highly unlikely that both distort the response in the same way and both are being used within the manufacturers' specified ranges of linear assessment.

D. Linear summation vs acoustically summed focus waves

A traditional TR experiment (meaning clipping TR was not used here) was conducted comparing a linear sum of the focal signals from each of the eight loudspeakers generated one at a time and summed in post processing, and the acoustically summed focus resulting from the energy focused by all eight loudspeakers simultaneously. This experiment was performed with the G.R.A.S. 46BG microphone positioned in the reverberation chamber away from any reflecting surfaces. A TRIR for each loudspeaker is generated individually as before, and then broadcast at increasing output levels for each loudspeaker individually. The maximum pressure amplitudes of each of the eight focus signals (each generated by one loudspeaker at a time) for each level is then linearly summed and compared to the levels measured when all eight loudspeakers are broadcasting their respective TRIRs simultaneously. A comparison of the measurements is shown in Fig. 8.

The peak compressions of the simultaneously broadcast focus signals are clearly higher in amplitude than the focus signals that were broadcast individually and then summed. This indicates that there is a nonlinear acoustic phenomenon by which the compression peaks are increasing nonlinearly as the output levels are increased. The same can be seen in the absolute value (magnitude) of the rarefaction measurements, indicating that the suppression of the rarefactions is stronger when the eight loudspeakers are used simultaneously versus when the singular measurements are summed. A threshold of where nonlinear gain becomes significant in the increase in the peak focus amplitude is set by the authors as occurring

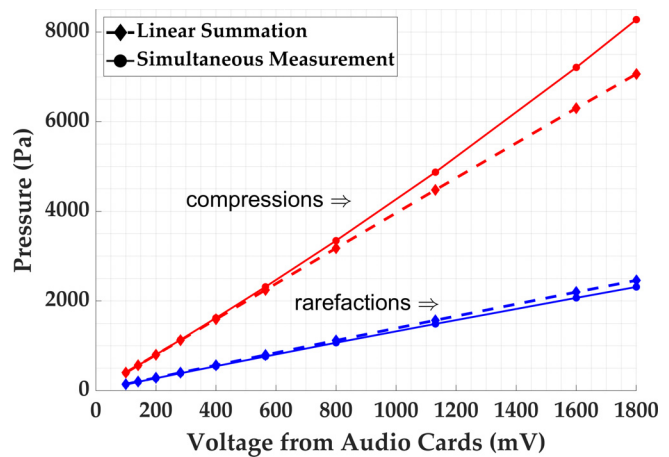


FIG. 8. (Color online) A comparison of the linearly summed peaks of focus signals generated by one loudspeaker at a time to the peak focus generated by all eight loudspeakers broadcasting simultaneously at increasing levels. The peak rarefaction values are represented as an absolute value of the measurement, and as such are positive. Traditional TR was used for these data.

when the ratio of the pressure between the simultaneously recorded peak, p_{sim} , and the peak calculated by linear summation, p_{lin} , has a level difference ≥ 0.5 dB,

$$Nonlinear\ Threshold = 20 * \log_{10} \left(\frac{p_{sim}}{p_{lin}} \right) \geq 0.5\ dB. \tag{1}$$

A level of increase of 0.5 dB has been deemed significant enough that it would lie outside of the potential for error in the measurement. Using this method, the nonlinear threshold in the preceding focus signals occurs above 800 mV of output from the audio generator cards. This corresponds to a sound pressure level in the simultaneously broadcast data of 165 dB_{pk}.

It is worth noting that the clipping TR method nonlinearly introduces additional high frequency content into the TRIR signal. However, once introduced to the TRIR signals, the same TRIR signals are broadcast from the loudspeakers for each increased signal level, so the clipping TR process cannot be the cause of the increasing nonlinearity observed with increasing levels. To avoid the possibility of any nonlinearity induced through the use of clipping TR process itself, the preceding experiment was performed without applying the clipping method to the TRIR, i.e., using traditional TR. The nonlinear compression amplification and nonlinear rarefaction suppression effects still are present, though to a lesser degree because the focal amplitudes achieved were not as high. This confirms that it is the simultaneity of the converging acoustic waves that is contributing to the observed nonlinear increases. A clipping TR spectrum possesses high amplitudes at higher frequencies than a traditional TR spectrum but when the signal levels fed to the loudspeakers are increased, a nonlinear increase in those high frequency amplitudes is observed whether clipping TR or traditional TR is used. When the increasing amplitude experiment is repeated and the clipping method is applied,

the nonlinear threshold occurs at a much lower output level of 400 mV from the generator cards because clipping TR produces higher focal amplitudes. Which, when considering the nonlinear acoustic addition of high frequencies described above, is expected, corresponding to a sound pressure level of 173 dB_{pk}. This is the level reported by Willardson *et al.*²⁷ as the point at which nonlinearity was beginning to appear in the data when they applied the clipping method. Thus, when TR is performed with the clipping method, levels above 173 dB_{pk} can be considered to have significant nonlinear characteristics, whereas the threshold is 165 dB_{pk} for traditional TR. The difference in nonlinear thresholds of 8 dB seems to be related to the higher frequency content contained in a clipped TRIR relative to that in the traditional TRIR, suggesting that the nonlinear threshold depends on the frequency content, which makes sense.

A similar analysis of the highest peak amplitudes attained using clipping TR is done, showing that when all methods of high amplitude focus generation are applied [logarithmically weighted chirp signal, clipping TR process, and receiver placement near maximum number of reflecting surfaces in the room (corner)], the peak focus amplitude increases nonlinearly from linear expectations. It must be pointed out that the linear data by which the comparison is being made is purely an approximation of a linear sum, derived by using the equation of the line for the linear summation data in Fig. 8, and adjusted to begin at the initial data point of the high amplitude data set. But it also indicates significant nonlinear increases at and above 175 dB_{pk}. Figure 9 shows the results of this experiment, with the peak focus amplitudes plotted against the linear approximation, reaching a peak compression of 200.6 dB_{pk} at maximum output from the generator cards.

Squaring and summing the linearly scaled pressure values across the full duration of each signal length allows an estimation of the change in the potential energy of each signal with increasing focal amplitude. Figure 10 shows a lowering of overall potential energy in the scaled signals, despite the nonlinear increase observed in the main compression of the focal signal.

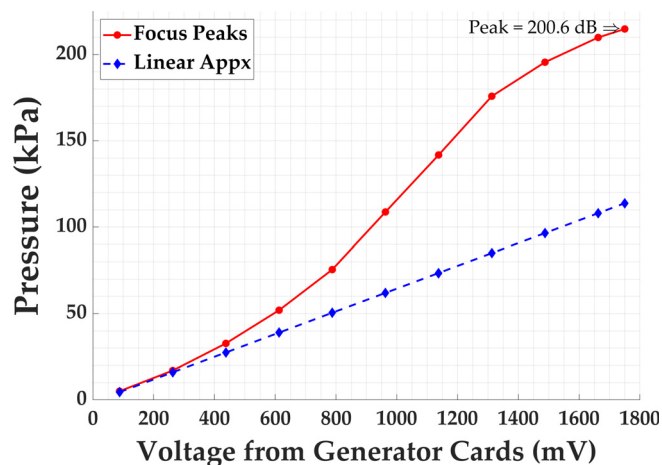


FIG. 9. (Color online) Peak focus amplitudes using clipping TR plotted alongside linearly scaled expected amplitudes.

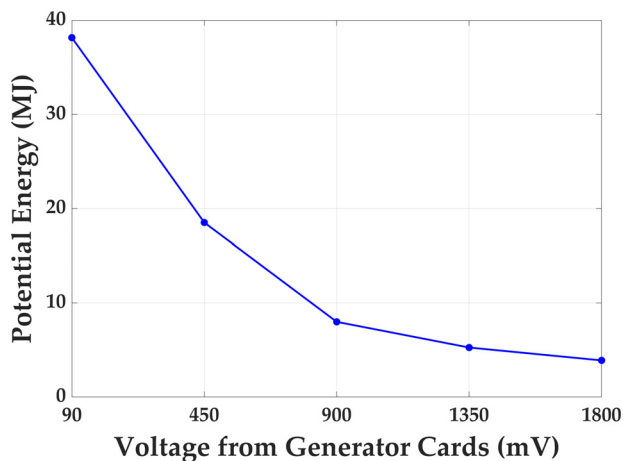


FIG. 10. (Color online) The sum of the potential energy values for the linearly scaled focal signals as the output from the generator cards is increased.

IV. LINE SCAN OF FOCUSING

A line scan of the spatial dependence of the high-amplitude TR focusing is presented in this section to obtain physical insights into the wave propagation during convergence and subsequent divergence in the TR focusing. This allows for a closer inspection of the changes to the converging and diverging waves as they propagate towards and away from the focal position, respectively. To conduct this experiment a linear-translation scanning system is placed in the larger reverberation chamber due to the size constraints of the smaller chamber. The experimental setup of the sources is similar to what was done previously in the smaller chamber. The PCB 112A23 microphone is mounted to an arm one meter above the ground, which is attached to the moving platform on the scanning system. The setup can be seen in Fig. 11.

IRs are obtained with the microphone at the center position of the scanning range. Once IRs are obtained, the microphone is moved 50 cm off of center and recordings are made across a line including the focal position from 50 cm to -50 cm in 0.50 cm increments, with the TRIRs being broadcast again for each microphone scan position. The

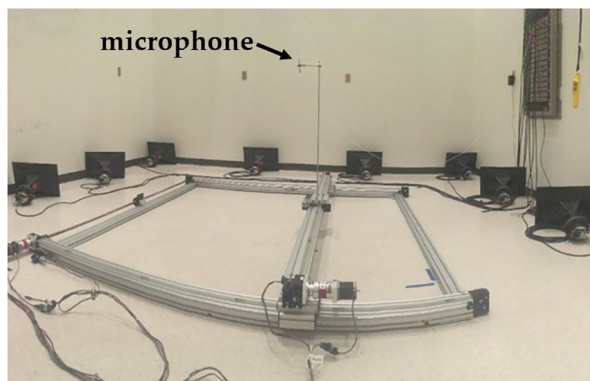


FIG. 11. (Color online) Photograph of the experimental layout for a one-dimensional line scan in the larger reverberation chamber. Distortion in the image is due to the panoramic nature of the photograph.

recordings at each position are then used to create an animation of the focused waves. The resulting animation (Mm. 1) shows waves approaching the focus location from both sides, the focusing moment, and waves moving away after the focus in one dimension. The duration of the entire animation represents 0.0068 s of time. Snapshots in time from this animation are depicted in Fig. 12.

Mm. 1. Animation of the spatial dependence of high-amplitude time reversal focusing over time. The data comes from a line scan in which the pressure was recorded at each spatial position while repeating the experiment. This is a file of type “.mp4” (4.34 MB).

Two important physical features may be observed in Mm. 1 and Fig. 12. The leading edge of the incoming wave fronts can be observed to steepen dramatically from Figs. 12(a) to 12(b). Figure 12(d) shows a time in which two waves are diverging outward after the focusing. The peak of the wave is visibly sharper in space relative to the incoming wave [compare the peaks in Figs. 12(b) and 12(d)]. This implies that there is more high frequency content in the

diverging waves than was present in the converging waves. This growth of high frequency content should be expected with wave steepening of high-amplitude propagating waves. Interestingly, in these two diverging waves it is now the trailing edge of both of these waves that is steeper. Normally one would expect that the two converging waves superpose and then pass through each other before and after focusing. This should result in the leading edges of both converging waves and diverging waves always being the steeper sides of the waves. The waves do not appear to reflect off of each other either since reflection would also result in the leading edge of the waves being steeper. A quantitative analysis of the converging waves shows that as the wave moves across the frame to the focus position from the outer edges, the wave speed, c , increases from approximately 373 m/s at the edges to approximately 526 m/s as it converges across the last 0.20 m to the focus. Using a binomial expansion of the adiabatic equation of state [$p = \gamma p_0 (\rho / \rho_0)$, where p is the acoustic pressure, γ is the ratio of specific heats, p_0 is the ambient pressure, ρ is the acoustic density, and ρ_0 is the ambient density], we can approximate the acoustic density of the air, ρ , as the wave passes the 0.10 m mark as 2.13 kg/m³, and a density of 2.64 kg/m³ at the time of focus. Using these values, the impedance of the converging waves just before they meet (at 0.10 m) is about 2.7 times higher than ambient conditions. Assuming adiabatic conditions hold, which is unlikely, the temperature, T_K , at the time of focus could be estimated ($T_K = c^2 / \gamma r$, where r is the specific gas constant). This would also suggest an instantaneous temperature at the focus of 690 K at the time of focus!

The full width half max of the peak is 4.5 ± 0.1 cm, with a peak amplitude in the line scan configuration of 188 dB_{pk}. This peak amplitude of the focusing is lower than the maximum value reported on in Fig. 4. This is due to the lack of rigid boundaries being near the focusing location (in order to allow for the scanning system hardware to be used) as expected from the work of Patchett *et al.*²⁹ The peak of the focusing in the line scan is 12 dB lower than when the focusing was in the corner of the room, whereas Patchett *et al.* suggested it should be closer to 9 dB lower between a corner location and a diffuse field location. It must be remembered that these two experiments of focusing to the corner and focusing for the line scan were done in different reverberation chambers. The line scan was done in the larger reverberation chamber, which chamber was also shown by Patchett *et al.* to reduce the peak amplitudes by an additional 3 dB. This means that the value of 12 dB lower than Fig. 4 is to be expected.

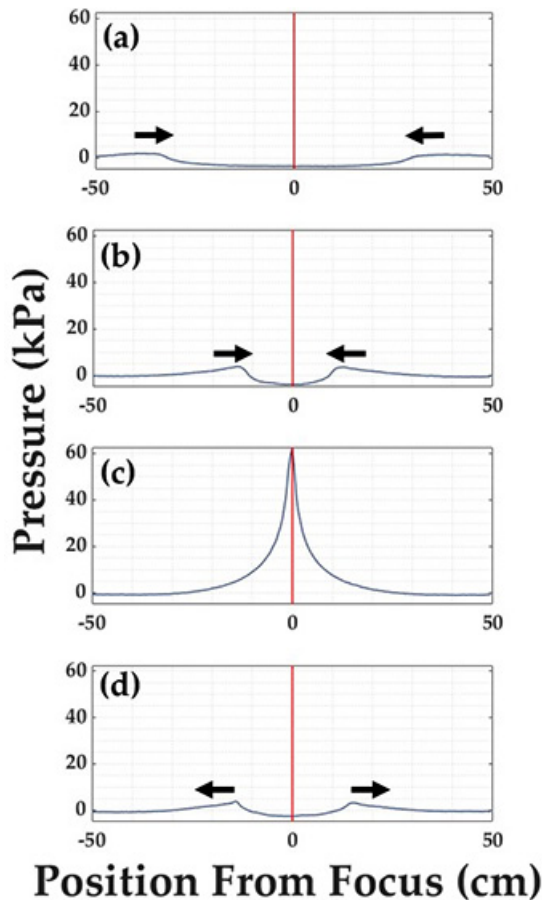


FIG. 12. (Color online) Snapshots in time from a spatial scan of the high-amplitude time reversal focusing. (a) Two waves converge toward the focal position. (b) The leading edge of each wave has steepened significantly as it progresses toward the focus. (c) The spatial dependence at peak focusing. (d) The trailing edge of each wave is steeper as they propagate away from the focus.

V. MACH STEM FORMATION IN CONVERGING WAVES

Ernst Mach first observed shockwave reflections in experiments reported in 1878.³⁶ It was noted that when a shockwave reflected from a rigid surface two types of phenomena could be observed. In the first, a shockwave propagates outward spherically from a source and is incident on a reflecting surface. The reflected wave and the incident wave

meet at the reflecting plane, and that intersection of the two propagates forward along the reflecting plane [Fig. 13(a)]. In the second, at a high enough pressure amplitude, the incident shock wave changes the ambient temperature and pressure of the medium it leaves behind (a breakdown of adiabatic assumptions) just enough to increase the speed of the reflecting wave. This allows the reflected shock wave to merge with the incident shock wave forming what has become known as a Mach stem [Fig. 13(b)]. The result is that three shock fronts are present, the incident shock, the reflected shock, and the region of convergence of the two, or the Mach stem.^{36,37}

The Mach stem is the superposition of the incident and reflected waves and has a pressure value somewhat greater than the summation of the incident and reflected wave amplitudes. A study conducted by Karzova *et al.*³⁸ explored the formation of Mach stems from focused nonlinear acoustic beams. It was shown that the formation of underwater Mach stems could be achieved in free-space with no rigid reflecting surface, just the existence of two superposed nonlinear acoustic beams using a model based on a numerical solution to the Khokhlov-Zabolotskaya-Kuznetsov (KZK) equation.³⁹ Hansen *et al.*⁴⁰ was able to show through numerical calculation that two overlapping astrophysical bow-shock fronts generated between two propagating high-amplitude waves form a Mach stem in the region between them. In an unclassified technical report released by the U.S. Army Ballistic Research Laboratory, Reisler *et al.*⁴¹ cited a study known as DIPOLE WEST, where measurements were made of simultaneous and non-simultaneous multi-blast shockwave interference in the air. The results from those tests conclusively showed that two or more shockwaves that interfere with each other generate the same Mach stem type effect seen when the shockwaves are incident upon hard boundaries, but at their intersection regions in the medium. This effect, referred to as Mach wave coalescence, was recently defined for small incidence angles in jet noise by Willis *et al.*,⁴² where the increase in wave amplitude and propagation distance was observed experimentally. Vaughn *et al.*⁴³ confirmed this effect by quantifying an angle of incidence for nonlinear Mach wave

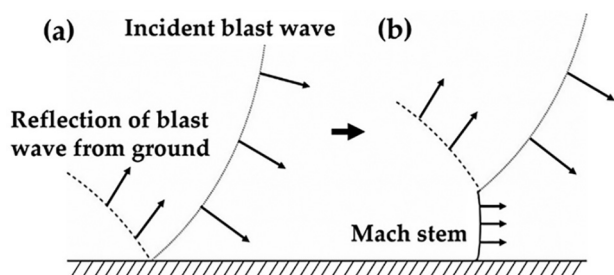


FIG. 13. Drawings of incident and reflected blast waves from an above ground explosion, along with a Mach stem formation. (a) The initial blast wave is incident on the ground, and the reflected wave propagates outward. (b) Later in time, and propagated further from the initial blast region in distance, the reflected wave and incident wave merge to form a Mach stem.

reflection leading to a steeper shock front at the reflecting surface.

These generated regions of excess pressures in the Mach wave front were greater than the sum of the initial waves combined. This supports a potential mechanism for the nonlinearly increased focal amplitudes of compressions observed in this paper. The amplitude of the time reversed waves continuously increases as the TRIRs are broadcast into the reverberation chamber at higher levels. As the final reflection paths converge to the focus, the propagation of sound coming from the walls to the microphone approximates an array of high-pressure spherical waves emanating from images sources that surround the focal position.^{25,44} As these waves converge to the focus, they begin to physically intersect with one another. At high-amplitudes it stands to reason that the overlapping areas of these waves reach a pressure level greater than their linear sum, due to free-space Mach stem formations. This effect is sketched in Fig. 14. Six of the many possible waves that contribute to the focusing are depicted to comprise the net spherically converging wave that creates the focus. At high-amplitudes Mach stems could be created at the overlapping regions of adjacent waves. If the reader will recall from the Introduction, Montaldo *et al.* showed that high-amplitude focusing did indeed generate wave steepening, but did not

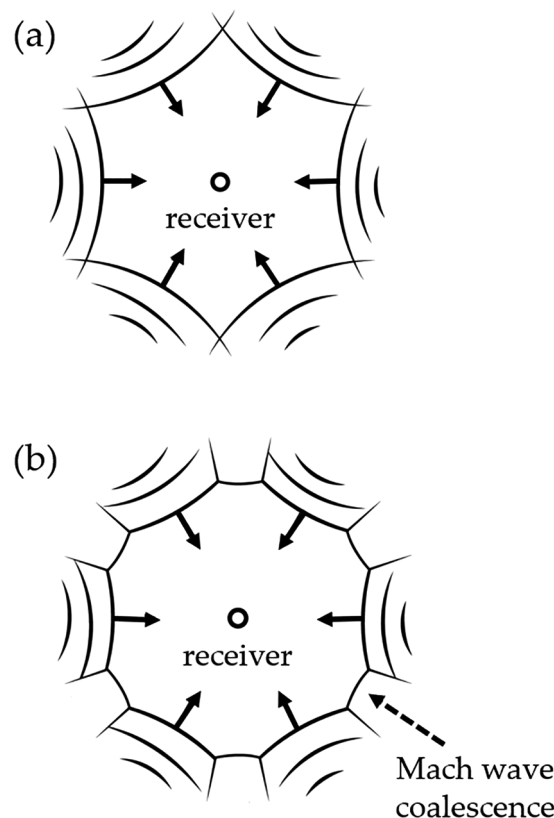


FIG. 14. (a) Drawing of six propagating waves that together approximate a spherically converging wave that arrives at the receiver position (or focal position). The arrows indicate the direction of travel of the wavefronts. (b) The overlapping regions form a Mach stem between them in free space, meaning there is no rigid reflecting surface necessary to generate the stem. One of the Mach stem regions is labeled for clarity.

show the nonlinear amplification of the compressions in the focusing as observed here. In that paper, underwater sound is being focused mainly from a single direction of propagation. This should result in fewer Mach stem formations since there are fewer overlapping waves converging to the focal location. Whereas, in the reverberation chamber the sound waves are coming in from all directions, allowing for a large quantity of overlapping regions and therefore increased opportunity for a free-space Mach stem effect to amplify the TR focusing nonlinearly.

VI. CONCLUSIONS

This paper reports a peak amplitude obtained through clipping TR focusing of audible sound in a reverberation chamber of 200.6 dB_{pk}. Significant nonlinear amplification of compressions by as much as a factor of 1.9 were observed, along with nonlinear suppression of rarefactions by as much as a factor of 2.1. Significant waveform steepening was observed in these high-amplitude focused waves as well. The initial observations of nonlinear phenomena reported by Willardson *et al.*²⁸ were much smaller deviations from predicted linearity. A threshold of nonlinearity can now be defined for applications of the traditional TR process of 165 dB_{pk}, and for the application of clipping TR of 173 dB_{pk}. This provides a benchmark value for an assumed linear or nonlinear regime of measurement.

This paper has shown evidence to support the idea that the nonlinear growth of focus amplitudes is genuine, along with the nonlinear suppression of rarefaction peaks. The application of TR focusing to generate such a large-amplitude signal has played a unique role in generating overlapping wave fronts by allowing for the convergence of these waves in a reverberant environment, and the nonlinear amplification is clearly evident at the levels attained. Autospectral analysis of the linearly scaled focus signals shows that there is a large increase in the high frequency content as the focus amplitude is increased, which is characteristic of nonlinear waveform steepening in the propagation of high amplitude waves. Both shock wave interaction theory, and experimental data presented here, leads us to believe that free-space Mach stems are being generated in the final converging waves of the TR process, which leads to the nonlinear increase in the peak focal compression amplitudes. This is because the focusing generates a wavefront that is the superposition of many converging high-amplitude waves upon each other. Future and ongoing experiments are seeking to verify this hypothesis of the Mach stems being the cause of the nonlinear increase in compression amplitudes. Thus, we believe that both nonlinear waveform steepening and nonlinear free-space Mach stem formation is occurring in high amplitude TR focusing of sound at the amplitudes reported.

¹M. Fink, "Time reversed acoustics," *Phys. Today* **50**(3), 34–40 (1997).

²B. E. Anderson, M. Griffa, C. Larmat, T. J. Ulrich, and P. A. Johnson, "Time reversal," *Acoust. Today* **4**(1), 5–16 (2008).

³B. E. Anderson, M. C. Remillieux, P.-Y. L. Bas, and T. J. Ulrich, "Time reversal techniques," in *Nonlinear Acoustic Techniques for Nondestructive Evaluation*, 1st ed., edited by T. Kundu (Springer, Berlin, 2018), Chap. 14, pp. 547–581.

⁴A. Parvulescu and C. S. Clay, "Reproducibility of signal transmissions in the ocean," *Radio Electron. Eng. U.K.* **29**(4), 223–228 (1965).

⁵C. S. Clay and B. E. Anderson, "Matched signals: The beginnings of time reversal," *Proc. Mtgs. Acoust.* **12**(1), 055001 (2011).

⁶S. Yon, M. Tanter, and M. Fink, "Sound focusing in rooms: The time-reversal approach," *J. Acoust. Soc. Am.* **113**(3), 1533–1543 (2003).

⁷J. V. Candy, A. W. Meyer, A. J. Poggio, and B. L. Guidry, "Time-reversal processing for an acoustic communications experiment in a highly reverberant environment," *J. Acoust. Soc. Am.* **115**(4), 1621–1631 (2004).

⁸G. Ribay, J. de Rosny, and M. Fink, "Time reversal of noise sources in a reverberation room," *J. Acoust. Soc. Am.* **117**(5), 2866–2872 (2005).

⁹J. V. Candy, D. H. Chambers, C. L. Robbins, B. L. Guidry, A. J. Poggio, F. Dowla, and C. A. Hertzog, "Wideband multichannel time-reversal processing for acoustic communications in highly reverberant environments," *J. Acoust. Soc. Am.* **120**(2), 838–851 (2006).

¹⁰B. Van Damme, K. Van Den Abeele, Y. Li, and O. Bou Matar, "Time reversed acoustics techniques for elastic imaging in reverberant and non-reverberant media: An experimental study of the chaotic cavity transducer concept," *J. Appl. Phys.* **109**(10), 104910 (2011).

¹¹B. E. Anderson, M. Clemens, and M. L. Willardson, "The effect of transducer directionality on time reversal focusing," *J. Acoust. Soc. Am.* **142**(1), EL95–EL101 (2017).

¹²M. Scalerandi, A. S. Gliozzi, C. L. E. Bruno, and K. Van Den Abeele, "Nonlinear acoustic time reversal imaging using the scaling subtraction method," *J. Phys. D: Appl. Phys.* **41**(21), 215404 (2008).

¹³M. Scalerandi, A. S. Gliozzi, C. L. E. Bruno, D. Masera, and P. Bocca, "A scaling method to enhance detection of a nonlinear elastic response," *Appl. Phys. Lett.* **92**(10), 101912 (2008).

¹⁴T. J. Ulrich, A. M. Sutin, T. Claytor, P. Papin, P.-Y. L. Bas, and J. A. TenCate, "The time reversed elastic nonlinearity diagnostic applied to evaluation of diffusion bonds," *Appl. Phys. Lett.* **93**(15), 151914 (2008).

¹⁵B. E. Anderson, M. Griffa, T. J. Ulrich, P.-Y. L. Bas, R. A. Guyer, and P. A. Johnson, "Crack localization and characterization in solid media using time reversal techniques," in *Proceedings of the 44th U.S. Rock Mechanics Symposium and 5th U.S.-Canada Rock Mechanics Symposium*, paper No. ARMA-10-154 (2010).

¹⁶P.-Y. Le Bas, M. C. Remillieux, L. Pieczonka, J. A. Ten Cate, B. E. Anderson, and T. J. Ulrich, "Damage imaging in a laminated composite plate using an air-coupled time reversal mirror," *Appl. Phys. Lett.* **107**(18), 184102 (2015).

¹⁷B. E. Anderson, L. Pieczonka, M. C. Remillieux, T. J. Ulrich, and P.-Y. L. Bas, "Stress corrosion crack depth investigation using the time reversed elastic nonlinearity diagnostic," *J. Acoust. Soc. Am.* **141**(1), EL76–EL81 (2017).

¹⁸S. M. Young, B. E. Anderson, S. M. Hogg, P.-Y. L. Bas, and M. C. Remillieux, "Nonlinearity from stress corrosion cracking as a function of chloride exposure time using the time reversed elastic nonlinearity diagnostic," *J. Acoust. Soc. Am.* **145**(1), 382–391 (2019).

¹⁹F. Ciampa and M. Meo, "Nonlinear elastic imaging using reciprocal time reversal and third order symmetry analysis," *J. Acoust. Soc. Am.* **131**(6), 4316–4323 (2012).

²⁰T. J. Ulrich, B. E. Anderson, P.-Y. L. Bas, C. Payan, J. Douma, and R. Snieder, "Improving time reversal focusing through deconvolution: 20 questions," *Proc. Mtgs. Acoust.* **16**, 045015 (2012).

²¹J.-L. Thomas, F. Wu, and M. Fink, "Time reversal focusing applied to lithotripsy," *Ultrason. Imag.* **18**(2), 106–121 (1996).

²²M. Tanter, J.-L. Thomas, and M. Fink, "Focusing and steering through absorbing and aberrating layers: Application to ultrasonic propagation through the skull," *J. Acoust. Soc. Am.* **103**(5), 2403–2410 (1998).

²³J.-L. Thomas and M. Fink, "Ultrasonic beam focusing through tissue inhomogeneities with a time reversal mirror: Application to transskull therapy," *IEEE Trans. Ultrason. Ferroelectr. Freq. Control* **43**(6), 1122–1129 (1996).

²⁴S. Dos Santos and Z. Prevorovsky, "Imaging of human tooth using ultrasound based chirp-coded nonlinear time reversal acoustics," *Ultrasonics* **51**(6), 667–674 (2011).

²⁵M. H. Denison and B. E. Anderson, "Time reversal acoustics applied to rooms of various reverberation times," *J. Acoust. Soc. Am.* **144**(6), 3055–3066 (2018).

- ²⁶M. H. Denison and B. E. Anderson, “The effects of source placement on time reversal focusing in rooms,” *Appl. Acoust.* **156**, 279–288 (2019).
- ²⁷M. L. Willardson, B. E. Anderson, S. M. Young, M. H. Denison, and B. D. Patchett, “Time reversal focusing of high amplitude sound in a reverberation chamber,” *J. Acoust. Soc. Am.* **143**(2), 696–705 (2018).
- ²⁸C. B. Wallace and B. E. Anderson, “High-amplitude time reversal focusing of airborne ultrasound to generate a focused nonlinear difference frequency,” *J. Acoust. Soc. Am.* **150**, 1411–1423 (2021).
- ²⁹B. D. Patchett, B. E. Anderson, and A. D. Kingsley, “The impact of room location on time reversal focusing amplitudes,” *J. Acoust. Soc. Am.* **150**, 1424–1433 (2021).
- ³⁰C. Appert, C. Tenaud, X. Chavanne, S. Balibar, F. Caupin, and D. d’Humières, “Nonlinear effects and shock formation in the focusing of a spherical acoustic wave,” *Eur. Phys. J. B* **35**, 531–549 (2003).
- ³¹G. Montaldo, P. Roux, A. Derode, C. Negreira, and M. Fink, “Ultrasound shock wave generator with one-bit time reversal in a dispersive medium, application to lithotripsy,” *Appl. Phys. Lett.* **80**, 897–899 (2002).
- ³²S. M. Young, B. E. Anderson, M. L. Willardson, P. E. Simpson, and P.-Y. L. Bas, “A comparison of impulse response modification techniques for time reversal with application to crack detection,” *J. Acoust. Soc. Am.* **145**(5), 3195–3207 (2019).
- ³³C. Heaton, B. E. Anderson, and S. M. Young, “Time reversal focusing of elastic waves in plates for educational demonstration purposes,” *J. Acoust. Soc. Am.* **141**(2), 1084–1092 (2017).
- ³⁴R. T. Beyer, *Nonlinear Acoustics* (Acoustical Society of America, Woodbury, NY, 1997), pp. 91–164, 165–203, 299–333.
- ³⁵C. E. Needham, *Blast Waves* (Springer, New York, 2010), pp. 19–22.
- ³⁶E. Mach, “Über den Verlauf von Funkenwellen in der Ebene und im Raume” (“Over course radiowaves plane space,”) *Sitzungsbr. Akad. Wiss. Wien* **78**, 819–838 (1878).
- ³⁷G. Ben-Dor, *Shock Wave Reflection Phenomena* (Springer Verlag, New York, 1992), pp. 3–13.
- ³⁸M. M. Karzova and V. A. Khokhlova, “Mach stem formation in reflection and focusing of weak shock acoustic pulses,” *J. Acoust. Soc. Am.* **137**(6), EL436–EL442 (2015).
- ³⁹J. N. Tjøtta and S. Tjøtta, “Nonlinear equations of acoustics, with application to parametric acoustic arrays,” *J. Acoust. Soc. Am.* **69**(6), 1644–1652 (1981).
- ⁴⁰E. C. Hansen, A. Frank, P. Hartigan, and K. Yirak, “Numerical simulations of Mach stem formation via intersecting bow shocks,” *High Energy Density Phys.* **17**, 135–139 (2015).
- ⁴¹R. E. Reisler, L. W. Kennedy, and J. H. Kefer, “High explosive multiburst airblast phenomena (simultaneous and non-simultaneous detonations),” U.S. Army armament research and development command: Ballistic Research Laboratory, technical report (Department of Commerce, Springfield, VA), <https://apps.dtic.mil/dtic/tr/fulltext/u2/a068462.pdf> (1979) (Last viewed March 10, 2021).
- ⁴²W. A. Willis III, C. E. Tinney, M. F. Hamilton, and J. M. Cormack, “Reduced-order models of coalescing Mach waves,” *AIAA SCITECH 2022 Forum*, AIAA 2022-1792 (2021).
- ⁴³A. B. Vaughn, K. M. Leete, K. L. Gee, B. R. Adams, and J. M. Downing, “Evidence for nonlinear reflections in shock-containing noise near high-performance military aircraft,” *J. Acoust. Soc. Am.* **149**(4), 2403–2414 (2021).
- ⁴⁴B. E. Anderson, T. J. Ulrich, and P.-Y. L. Bas, “Comparison and visualization of the focusing wave fields of various time reversal techniques in elastic media,” *J. Acoust. Soc. Am.* **134**(6), EL527–EL533 (2013).